



Hadron structure from lattice QCD

C. Alexandrou^{a,b}, K. Jansen^c^a*Department of Physics, University of Cyprus, P.O. Box 20537, 1678 Nicosia, Cyprus*^b*Computation-based Science and Technology Research Center, The Cyprus Institute, 20 Kavafi Str., Nicosia 2121, Cyprus*^c*John von Neumann-Institute for Computing, DESY, Platanenallee 6, D-15738 Zeuthen, Germany*

Abstract

We review results for hadron masses and hadron structure using maximally twisted mass fermions for our non-perturbative studies of lattice QCD. We demonstrate that hadron masses can be computed reliably in this setup and that a nice agreement with the experimentally determined spectra is found. In addition, we give examples that lattice QCD can also provide predictions of masses for a number of yet not discovered states. We present a number of results for moments of parton distribution functions and form factors and show that simulations at the physical value of the pion mass have the promising potential to reconcile older discrepancies between lattice results and those from experiment or phenomenology. In addition, we show that it is also possible to include dis-connected quark loop contributions in the analysis when a large enough statistics is invested. Finally, we give an outlook for future lattice calculations of hadron structure by discussing the gluon moment, first results of a direct computation of the parton distribution functions and mention the neutron electric dipole moment.

Keywords: Lattice QCD, hadron spectrum, moments of parton distribution functions, dis-connected quark loops, nucleon form factors

1. Introduction

Although our theory of the strong interaction, quantum chromodynamics (QCD), predicts the existence of quarks and gluons, they cannot be observed as free particles. Instead, we only observe bound states, the hadrons. However, through deep inelastic scattering experiments it is possible to reveal the structure of hadrons and to provide us fascinating insight in the interactions of quarks and gluons. This leads to a much better understanding of the structure of matter and also enhances our knowledge of the universe today and in its early stages. The structure of hadrons is described by parton distribution functions (PDFs) which provide information on the distributions of the different quarks and gluons in a hadron, their momentum, angular momentum and spin, see [1].

In a standard analysis, the PDFs are parametrized phenomenologically. In addition, the necessary renormalization of the PDFs is performed perturbatively.

This prevents a direct, first principle prediction of the PDFs from QCD alone. In principle, this somewhat unsatisfactory situation could be overcome by non-perturbative lattice calculations, but on the lattice the PDFs cannot be computed directly. The reason is that light-cone dynamics is needed and going to short, or even zero distance on the Euclidean space-time lattice QCD is not possible. See, however, the discussion at the end of this contribution for a proposal to compute PDFs directly.

The key, how lattice QCD can nevertheless contribute to obtain non-perturbative information on hadron structure is the operator product expansion which allows to express the PDFs in terms of matrix elements of local operators which are accessible to lattice QCD calculations. In this way, not the PDFs themselves are analyzed, but moments of them are computed which themselves can be compared to experiment or phenomenological analyses. In this contribution to the proceedings

of the Transregional Collaborative Research Center 9 “Computational Particle Physics” we will report on the status of hadron masses and hadron structure calculations and discuss results that emerged from this work. For a broader discussion and introductions to the subject, we refer to the excellent reviews [2, 3, 4, 5, 6, 7].

As a main result of this contribution we remark already here that very recent calculations performed at a physical value of the pion mass show a very promising tendency to reconcile older discrepancies between lattice results and experimental or phenomenological ones, see also the recent reviews of refs. [8, 9, 10, 11]. We will demonstrate the progress that has been achieved at the examples of the axial charge and the average quark momentum of the nucleon. We will also discuss baryon form factors, the nucleon σ -terms and non-perturbative renormalization for which we devoted a dedicated effort.

Another area where substantial progress has been made on the lattice are the calculations of singlet, disconnected quark loop contributions. Here, through special techniques and investing a very high statistics, a quantitative evaluation of many dis-connected contributions could be obtained going thus far beyond the standard a few years ago. We will close this contribution showing first results for the so far unexplored gluon, discuss a proposal to compute PDFs directly on the lattice and attempt to evaluate the neutron electric dipole moment as a most promising quantity to detect new physics beyond the standard model.

The work discussed here is closely linked to [12] where a perturbative, phenomenological analysis has been carried out. Numerous discussions and scientific exchanges furthered both projects substantially and focused the calculations on the most important hadron structure quantities and questions where both approaches have contributed in a common approach.

In the following, we will start with a discussion of the structure of the pion which has been the main focus in the initial stage of this project. We will then move to hadron masses before we show the remarkable progress in the computation of dis-connected quark loop contributions that was made during the duration of this project. After discussing aspects of non-perturbative renormalization, we will then move to moments of parton distribution functions and form factors before we conclude and provide an outlook for further very promising developments.

2. Lowest moment of the pion

A first benchmark quantity to be studied with lattice computations is the average quark momentum in a pion as the lowest moment of a non-singlet quark distribution function. In the pioneering work of reference [13] it has been demonstrated that calculations of such a low lying moment is indeed feasible. However, such calculations, carried through in the quenched approximation in the past, had additionally to be performed at large, unphysical values of the pion mass and therefore a chiral extrapolation becomes necessary. A major obstacle has been that the used pion masses were as large as 500 MeV making such extrapolations very difficult and hard to control, see refs. [14, 15, 16, 17, 18, 19].

In the contribution [20] it has been demonstrated for the case of, e.g., the pion decay constant that with maximally twisted mass fermions [21] much smaller pion masses can be reached. It is therefore very tempting to also perform a calculation of the average quark momentum with twisted mass fermions. The first target observable has been a twist-2 operator, which is related to the the lowest moment $\langle x \rangle$ of the quark parton distribution function in a pion.

The twist-2 operators have the following expressions

$$O_{\mu_1 \dots \mu_N}^a(x) = \frac{1}{2^{N-1}} \bar{\psi}(x) \gamma_{\{\mu_1} \overleftrightarrow{D}_{\mu_2} \dots \overleftrightarrow{D}_{\mu_N\}} \frac{1}{2} \tau^a \psi(x), \quad (1)$$

with $\{\dots\}$ the symmetrization on the Lorentz indices and

$$\overleftrightarrow{D}_\mu = \overrightarrow{D}_\mu - \overleftarrow{D}_\mu; \quad D_\mu = \frac{1}{2} [\nabla_\mu + \nabla_\mu^*]. \quad (2)$$

The Pauli matrices τ^a are used to act in flavour space. For details, how to treat such operators for twisted mass fermions, we refer to ref. [22]. The lowest moment for the up (or down) quark can be expressed as

$$O_{\mu\nu}^u(x) = \frac{1}{2} \bar{\psi}(x) \gamma_{\{\mu} \overleftrightarrow{D}_{\nu\}} \frac{(1 + \tau^3)}{2} \psi(x) - \delta_{\mu\nu} \cdot \text{trace terms}. \quad (3)$$

There are two representations of such a non-singlet operator on the lattice [23, 24] and we choose

$$O_{44}^u(x) = \frac{1}{2} \bar{\psi}(x) \left[\gamma_4 \overleftrightarrow{D}_4 - \frac{1}{3} \sum_{k=1}^3 \gamma_k \overleftrightarrow{D}_k \right] \frac{(1 + \tau^3)}{2} \psi(x), \quad (4)$$

since in this form we can work at zero external momentum which gives a better signal to noise behaviour.

For the computation of the matrix elements of this operator we follow refs. [25, 13]. To this end, we write

$$P^\pm(x) = \bar{\psi}(x)\gamma_5 \frac{\tau^\pm}{2} \psi(x), \quad \tau^\pm = \frac{\tau^1 \pm i\tau^2}{2} \quad (5)$$

as the required interpolating operator. The ratio of the 3-point function

$$C_{44}(y_4) = a^6 \sum_{\mathbf{x}, \mathbf{y}} \langle P^+(0) \mathcal{O}_{44}(\mathbf{y}, y_4) P^-(\mathbf{x}, T/2) \rangle, \quad (6)$$

and the 2-point function

$$C_P(x_4) = a^3 \sum_{\mathbf{x}} \langle P^+(0) P^-(\mathbf{x}, x_4) \rangle, \quad (7)$$

will then provide the matrix element we are interested in which can be derived by performing a transfer matrix decomposition. Defining

$$R(y_4) = \frac{C_{44}(y_4)}{C_P(T/2)}, \quad (8)$$

we can look for a plateau in the large Euclidean time y_4 limit where this ratio takes the form

$$\langle 0, PS | \mathcal{O}_{44} | 0, PS \rangle = 2m_{PS} R, \quad (9)$$

where $|0, PS\rangle$ represents the pion state. From this relation we can extract the bare matrix element

$$\langle x \rangle^{\text{bare}} = \frac{1}{m_{PS}} \cdot R. \quad (10)$$

This bare matrix element needs a multiplicative renormalization factor for which we take the renormalization group invariant renormalization constant Z_{RGI} as computed in refs. [19, 17] from a Schrödinger functional (SF) renormalization scheme [26, 27, 28, 29]. In this way, a well defined continuum limit can be performed and in the $\overline{\text{MS}}$ scheme, typically used in phenomenology, the renormalized matrix element reads

$$\langle x \rangle^{\overline{\text{MS}}}(\mu, r_0 m_{PS}) = \lim_{a \rightarrow 0} \frac{\langle x \rangle^{\text{bare}}(a, m_{PS}) Z_{\text{RGI}}(a)}{f^{\overline{\text{MS}}}(\mu)} \quad (11)$$

where the renormalization scale is given at $\mu = 2 \text{ GeV}$ and $f^{\overline{\text{MS}}}(\mu)$ is taken from ref. [19].

In fig. 1 we show the so obtained renormalized matrix element of the pion as a function of the pion mass. As the graph demonstrates, with twisted mass fermions indeed smaller values of the pion mass could be reached than it was possible with standard Wilson or clover improved Wilson fermions.

As fig. 1 indicates, the lattice data move with decreasing pion mass towards the phenomenological result. However, it is clear that two major improvements

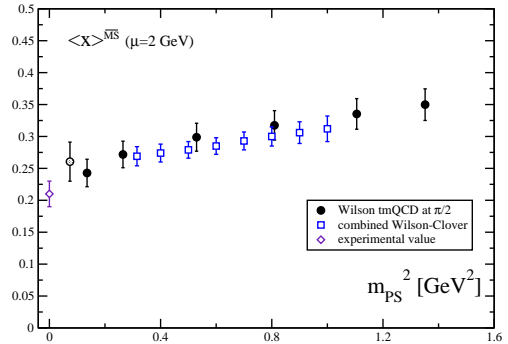


Figure 1: The average quark momentum in the pion, $\langle x \rangle^{\overline{\text{MS}}}(\mu = 2 \text{ GeV})$, in the continuum limit as a function of the pion mass. The squares represent results from Wilson and clover improved Wilson simulations [19]. The circles are from twisted mass fermions. The diamond represents the phenomenologically extracted value from refs. [30, 31]. There is also a result from ref. [32] which reads $\langle x \rangle^{\overline{\text{MS}}}(\mu = 2.28 \text{ GeV}) = 0.217(11)$.

would be highly desirable. The first one is to leave the quenched approximation and to include the light quarks as active degrees of freedom in the simulations. The second improvement should be to perform calculations directly at a physical value of the pion mass in order to avoid extrapolations. At the time when the results of ref. [22] were published it was thought that these steps were extremely difficult, if not impossible, to surmount in the near future.

However, as outlined in [20], within the twisted mass setup, new algorithms were developed [33, 34] which, together with substantial advances of supercomputers, made it possible to perform simulations directly at the physical point with active light quarks. In fig. 2 we show a recent calculation of the average quark momentum in a pion performed with $N_f = 2$ flavours of maximally twisted mass fermions, see also [35, 36].

Although for the data point at the physical pion mass systematic effects from the lattice spacing and the finite volume are not yet available, the graph is very promising in reconciling earlier discrepancies between lattice and phenomenological results.

3. Baryon masses

One important expectation we have from QCD as our theory of the strong interaction is that it explains the spectrum of bound states, in particular the baryon

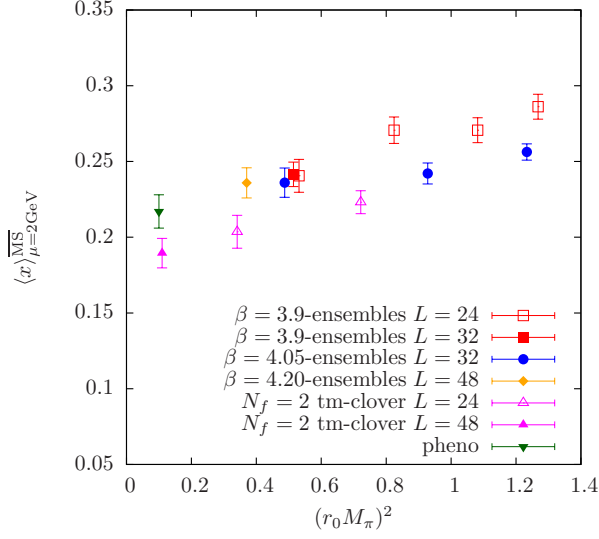


Figure 2: The average quark momentum in the pion for $N_f = 2$ flavours of active light quarks. We show data from simulations at quark masses larger than the physical ones and also from a recent calculation performed directly at the physical point.

masses. Here, due to the confinement of quarks, non-perturbative methods are mandatory and lattice QCD should be an ideal tool to address the baryon spectrum. In [20] we have already shown the light baryon spectrum as computed for $N_f = 2 + 1 + 1$ flavours of quarks in ref. [37]. An earlier calculation for $N_f = 2$ flavours of mass-degenerate light quarks has been performed in refs. [38, 39], see also ref. [40] for a recent review. Here, we want to concentrate on charmed baryons which will lead in the end even to predictions for certain baryon masses.

In order to extract baryon masses correlation functions of suitable operators are taken at zero momentum, $\vec{p} = \vec{0}$. Such correlation functions read in general

$$C_X^\pm(t, \vec{p} = \vec{0}) = \sum_{\Delta\mathbf{x}} \langle \frac{1}{2} \text{Tr} P_\pm \mathcal{J}_X(\mathbf{x}_{\text{sink}}, t_{\text{sink}}) \bar{\mathcal{J}}_X(\mathbf{x}_{\text{source}}, t_{\text{source}}) \rangle \quad (12)$$

with $\Delta\mathbf{x} = \mathbf{x}_{\text{sink}} - \mathbf{x}_{\text{source}}$, $P_\pm = \frac{1}{2} 1 \pm \gamma_0$, $t = t_{\text{sink}} - t_{\text{source}}$ and \mathcal{J}_X the operator corresponding to the particular baryon. The correlation function is evaluated between the source point $(\mathbf{x}_{\text{source}}, t_{\text{source}})$ and the sink point, $(\mathbf{x}_{\text{sink}}, t_{\text{sink}})$. Utilizing the symmetries in Euclidean time [37], we construct

$$C_X(t) = C_X^+(t) - C_X^-(T - t). \quad (13)$$

The ground state mass of a given hadron can be ex-

tracted by examining the effective mass defined by

$$\begin{aligned} am_{\text{eff}}^X(t) &= \log\left(\frac{C_X(t)}{C_X(t+1)}\right) \\ &= am_X + \log\left(\frac{1 + \sum_{i=1}^{\infty} c_i e^{-\Delta_i t}}{1 + \sum_{i=1}^{\infty} c_i e^{-\Delta_i(t+1)}}\right) \\ &\rightarrow_{t \rightarrow \infty} am_X \end{aligned} \quad (14)$$

where $\Delta_i = m_i - m_X$ is the mass difference of the excited state i with respect to the ground mass m_X . All results in this work have been extracted from correlators where Gaussian smearing is applied both at the source and the sink. The sum over excited states in the effective mass given in eq. (14) is truncated, keeping only the first excited state,

$$am_{\text{eff}}^X(t) \approx am_X + \log\left(\frac{1 + c_1 e^{-\Delta_1 t}}{1 + c_1 e^{-\Delta_1(t+1)}}\right). \quad (15)$$

The upper fitting time slice boundary is kept fixed, while allowing the lower fitting time to be two or three time slices away from t_{source} . We then fit the effective mass to the form given in eq. (15). This exponential fit yields an estimate for c_1 and Δ_1 as well as for the ground state mass, which we denote by $m_X^{(E)}$. Then, we perform a constant fit to the effective mass increasing the initial fitting time t_1 . In this way, we have determined the full octet and decuplet baryon mass spectra, see ref. [37] for further details. In figs. 3 and 4 we show the charm baryon spectra we have obtained. As can be seen, there is a nice agreement with the experimentally found spectra and we can even give predictions for the mass for the not yet detected doubly charmed Ξ_{cc}^* and the doubly and triply charmed Ω s.

4. Nucleon structure: nucleon axial charge and average quark momentum

The last section demonstrated that lattice QCD can successfully reproduce the baryon spectrum and even provides predictions for the masses of certain, not yet experimentally detected states. This great achievement suggests that –similar as in the case of the structure of the pion discussed above– also the structure of nucleons could be explored. Indeed, there is a large activity over the last decades to address nucleon structure, see e.g. [2, 3, 4, 5, 6, 7] and the recent reviews of refs. [8, 9, 10, 11]. In all these works, as in the case for pion parton distribution functions (PDF), moments of the PDF are calculated. The prime targets have been the axial charge of the nucleon g_A , the average quark momentum in the nucleon and the nucleon charge radius. The computations of these quantities have been

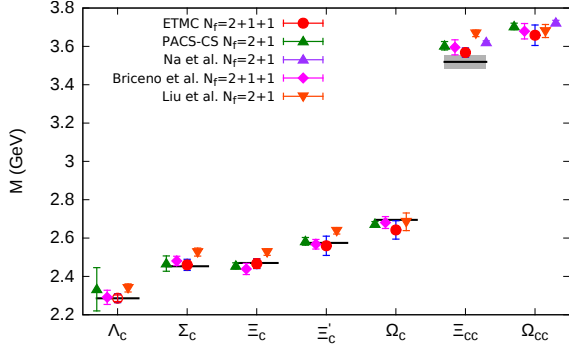


Figure 3: The spin-1/2 charm baryon masses are shown together with the experimental masses [41] represented by the horizontal bands. Included are results from various groups using staggered quarks [42, 43] (purple triangles), [44] (magenta diamonds) and [45] (orange inverted triangles). Results from PACS-CS [46] are shown in green triangles. For the twisted mass results of this work (red circles) the chiral extrapolation was performed using the leading order HB χ PT. In our results, the statistical error is shown in red, whereas the blue error bar includes the statistical error and the systematic errors due to the chiral extrapolation and due to the tuning added in quadrature.

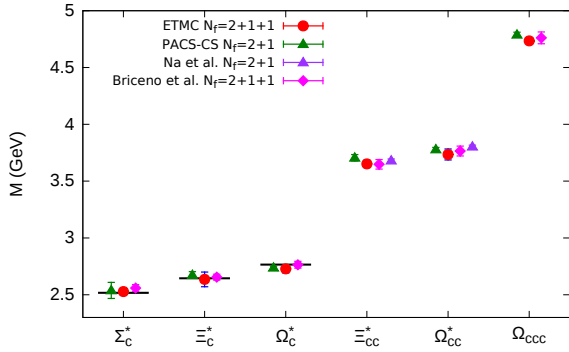


Figure 4: The spin-1/2 charm baryon masses are shown together with the experimental masses [41] shown by the horizontal bands. The notation is the same as in fig. 3.

performed in the past at unphysically large pion masses and have been reviewed in refs. [4, 5, 6, 7] where it was demonstrated that there are severe discrepancies between results from lattice QCD calculations and experimental or phenomenological extractions of these moments.

However, there are indications that with simulations directly at the physical pion mass, taking systematic errors into account and also including dis-connected contributions (when necessary) these discrepancies tend to vanish [8, 9, 10, 11]. In the following, we want to address the just mentioned aspects of systematic effects, physical point simulations and dis-connected contributions.

The zero momentum nucleon 2-point correlation

function on the lattice is defined in eq. (12) and reads

$$C_2(t) = \Gamma_{\alpha\alpha'} \sum_{\vec{x}} \langle J_{N,\alpha'}(\vec{x}, t) \bar{J}_{N,\alpha}(0) \rangle \quad (16)$$

where \bar{J}_N is a nucleon interpolating field

$$J_{N,\alpha}(x) = \varepsilon^{abc} u_\alpha^a(x) \left((d^b(x))^T C \gamma_5 u^c(x) \right), \quad (17)$$

where $C = i\gamma_0\gamma_2$ is the charge conjugation operator.

Similarly to the case of the pion 3-point function of eq. (6) we need the corresponding 3-point function for the nucleon to compute the matrix element of interest,

$$C_3(t, t') = \Gamma'_{\alpha\alpha'} \sum_{\vec{x}, \vec{y}} \langle J_{N,\alpha'}(\vec{x}, t) \mathcal{O}(\vec{y}, t') \bar{J}_{N,\alpha}(\vec{0}, 0) \rangle, \quad (18)$$

where \mathcal{O} is the desired local field of the operator $\hat{\mathcal{O}}$ and Γ' is a matrix in Dirac space related to the operator. By t' we denote the insertion time. Performing a transfer matrix decomposition of the 3-point function, we find

$$C_3(t, t') = \sum_{j,k} J_N^{(j)} \bar{J}_N^{(k)} e^{-m_j(t-t')} e^{-m_k t'} \langle j | \hat{\mathcal{O}} | k \rangle,$$

leading to the asymptotic large Euclidean time limit

$$\lim_{(t-t'), t' \rightarrow \infty} C_3(t, t') \rightarrow J_N^{(0)} \bar{J}_N^{(0)} e^{-m_N t} \langle 0 | \hat{\mathcal{O}} | 0 \rangle.$$

From this asymptotic behaviour the nucleon matrix element $\langle 0 | \hat{\mathcal{O}} | 0 \rangle$ is then obtained from the ratio of the 3-point and the 2-point function

$$\langle 0 | \mathcal{O} | 0 \rangle = \lim_{(t-t'), t' \rightarrow \infty} \frac{C_3(t, t')}{C_2(t)}. \quad (19)$$

The just sketched procedure to extract nucleon matrix elements assumes that the asymptotic Euclidean time limits can be reached such that only the ground state, i.e. the nucleon, contributes. In practice, of course, this asymptotic limit cannot be reached and excited states will have an effect on the extraction of the matrix element under consideration.

4.1. Excited state effects

It has been a suspicion that, in fact, these excited state contaminations could be responsible for the discrepancy between lattice results and experimental or phenomenological extractions of moments of PDFs. The problem for lattice computations is that with growing times $t - t'$ and t' the signal to noise ratio becomes worse and worse. With a statistics of standard lattice calculations of a few hundred measurements, it is thus very difficult,

if not impossible, to detect excited states effects. As a serious attempt to address the question of excited state contaminations, we have performed a benchmark computation [47] by increasing the statistics by at least an order of magnitude. This led for the first time to a quantitative estimate of the values of $t - t'$ and t' which need to be taken in order to not suffer from these excited state contaminations.

The key ingredient is again a transfer matrix decomposition of the ratio of the 3-point and the 2-point functions and, considering only the first excited state, one finds

$$\begin{aligned} \frac{C_3(t, t')}{C_2(t)} &= \langle 0 | O | 0 \rangle \\ &+ \langle 0 | O | 1 \rangle \frac{\bar{J}_N^{(1)}}{\bar{J}_N^{(0)}} \exp(-\Delta M t') \\ &+ \langle 1 | O | 0 \rangle \frac{J_N^{(1)}}{J_N^{(0)}} \exp[-\Delta M(t - t')] \\ &+ O[\exp(-\Delta M t)] , \end{aligned}$$

where ΔM is the mass gap between the nucleon ground state and the first excited state.

For our investigation, we have chosen the time slice of the operator insertion to be $t' = 9a$ in order to suppress excited state contributions from the source. In [47] we have also developed an *open source method* which allows to go to large Euclidean times without the need of performing new calculations for each new time value. This is advantageous over the standard fixed source method and made it possible to explore the excited state contaminations which has been the target of this work.

As a first quantity, we have studied the nucleon axial charge g_A for various source-sink separations. Clearly, from fig. 5 it can be seen that the value of g_A does not show any statistically significant dependence on the source-sink separation t . Hence, the plot demonstrates that there is no contribution from excited states detectable within the statistical accuracy of 2.5%. Note that for this analysis of g_A we have employed roughly 7500 measurements when we take $t = 18a$. In our standard analysis [48] we have typically used 500 measurements for $t = 12a$. The investigation performed here demonstrates that most probably excited state effects cannot explain the discrepancy between lattice and phenomenological results for g_A which therefore remains.

The second quantity that we have considered is the average quark momentum, $\langle x \rangle_{u-d}$. Our standard analysis is given in ref. [48]. For the case of $\langle x \rangle_{u-d}$ we have carried out in total about 23, 000 measurements us-

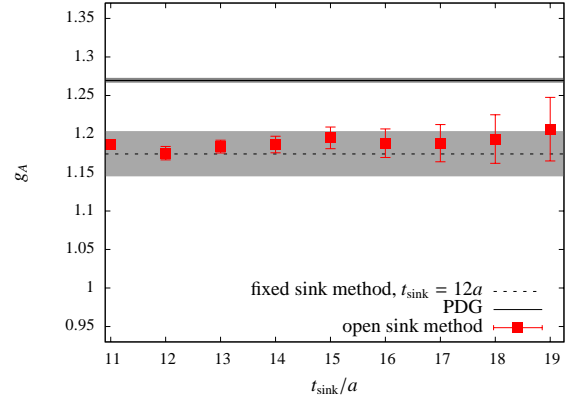


Figure 5: The dependence of g_A on the source-sink separations. The light gray band indicates the result obtained from an earlier calculation using a source-sink separation of $12a$ and the dark gray band shows the experimental value [49].

ing randomly distributed source points with 5 sources per configuration. This statistics led to a precision at a source-sink separation of $t = 18a$, which equals the one of the standard calculation with a source-sink separation of $t = 12a$ using 1300 measurements.

Fig. 6 shows $\langle x \rangle_{u-d}$ as a function of the source-sink separation t . The phenomenological result also shown in the graph is taken from ref. [50]. The standard calculation is taken from refs. [51, 52]. As can be seen in fig. 6 for the case of $\langle x \rangle_{u-d}$ excited state contaminations are visible. However, it needs to be stressed that the effect of excited states, although going in the right direction, is clearly not large enough to reconcile lattice results with phenomenological extractions of this quantity.

The dependence of $\langle x \rangle_{u-d}$ on t , can be estimated by fitting the expected exponential behavior,

$$\langle x \rangle_{u-d} + A \exp[-\Delta M(t - t')] , \quad (20)$$

to the lattice results with a fixed $t' = 11a$. From such a fit, we find that at infinite time $\langle x \rangle_{u-d} = 0.22(1)$, which is 12% lower than the result of $\langle x \rangle_{u-d} = 0.250(6)$, obtained using $t = 12a$ in the fixed sink method.

4.2. Dis-connected contributions

Another systematic effect that had been neglected in the past are dis-connected quark loops. It can be expected that for flavour singlet quantities these contributions cannot be neglected. The reason is that for flavour singlet quantities these contributions add up for the different flavours and given the accuracy the connected contributions can be computed presently, the dis-connected quark loops can give a non-negligible effect.

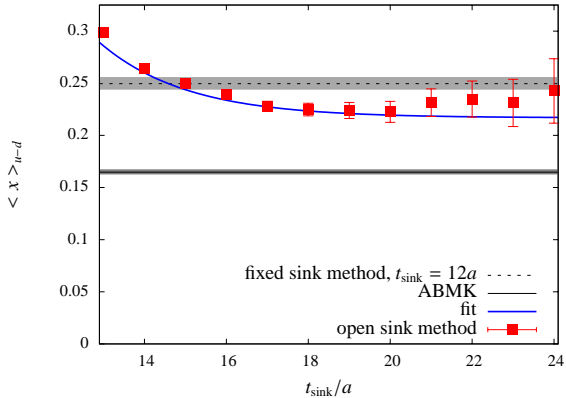


Figure 6: Results for the dependence of $\langle x \rangle_{U-d}$ on the source-sink separation. The operator has been inserted at $t' = 11a$. The value from the standard calculation at $t = 12a$ is indicated by the light gray band. The phenomenologically extracted value is shown with the dark gray band. The blue solid line corresponds to a fit of eq. (20) described in the text.

The problem of dis-connected quark loop computations in lattice QCD is that they require the calculation of all-to-all or time-slice-to-all propagators, which cannot be computed to a high precision given the computational resources available to a typical lattice QCD collaboration. In particular, to reach a comparable accuracy to the connected contributions a much larger computational effort is needed. As a consequence, in most lattice QCD calculations the disconnected contributions were neglected leaving us with an unknown systematic error.

There has been, however, a substantial improvement on the algorithmic side. This, in combination with new supercomputer architectures has made it possible to now address the dis-connected quark loops on a quantitative level. In ref. [53] we set out to perform a most comprehensive comparison of various algorithmic techniques in order to see, what is the optimal method to evaluate dis-connected quark loops. In addition, in many cases we performed about 150,000 measurements to obtain statistically significant results. The systematic investigation of different methods for various quantities and the enormous statistics we have reached set a new standard in the area of computing dis-connected quark loops for hadronic quantities and showed which effort needs to be invested to be able to estimate the dis-connected contributions in a statistically significant way.

To be more concrete, we tested the one-end trick [54, 55, 56], dilution [57, 58, 59, 60, 61], the Truncated Solver Method (TSM) [61, 62, 63] and the Hopping Parameter Expansion (HPE) [54, 64]. It is worth stressing

that the use of graphics cards (GPUs) are very advantageous for the computation of quark propagators and contractions needed for the dis-connected quark loop contributions [53, 65, 66]. In particular, when a large number of inversions on a given gauge field configuration is needed GPUs provide an optimal platform.

In table 1 we provide a comparison of the cost and the achieved error for the various algorithmic techniques and for a given quantity. For this comparison, we have fixed the number of measurements to about 20,000. This table can be used as a look-up table to infer which technique is best suited for a given observable. It provides the first comprehensive list of such an algorithmic comparison for dis-connected contributions.

Method	Abs. Error	OH	Cost	Cost \times Error ²
$\sigma_{\pi N}$				
One-end trick	4.3 MeV	65	2234	0.032
One-end trick + TSM	3.8 MeV	290	1471	0.027
σ_s				
One-end trick	5.1 MeV	65	754	0.019
One-end trick + TSM	4.9 MeV	409	809	0.019
Time-dil.	13 MeV	31	745	0.126
Time-dil. + TSM	7.5 MeV	281	710	0.040
Time-dil. + HPE	8.0 MeV	34	750	0.048
Time-dil. + HPE + TSM	6.2 MeV	322	750	0.029
g_A				
One-end trick	0.19	65	2234	80.6
One-end trick + TSM	0.081	409	1471	9.65
g_A^s				
One-end trick	0.076	65	754	4.36
One-end trick + TSM	0.023	409	809	0.43
Time-dil.	0.132	31	721	5.08
Time-dil. + TSM	0.049	281	676	1.62
Time-dil. + HPE	0.040	34	725	1.16
Time-dil. + HPE + TSM	0.024	322	692	0.40

Table 1: Comparison of the computational cost for the light and strange σ -terms and axial charges. The costs given in units of GPU-node seconds (2 GPUs per node). In order to compare the different techniques, we employed the same statistics, namely 18628 measurements. The column labeled as OH denotes the *overhead*, which is the time of pre- and post-processing for the computation of the dis-connected quark loops. The total cost includes, of course, also the inversion. The last column defines a quantity that is independent of statistics, which gives the comparative cost for a fixed error of a given observable [67]. For further details, we refer to ref. [53].

Equipped with the optimal computational technique to evaluate the dis-connected contribution for a given nucleon observable, we carried out a high statistics analysis of a number of nucleon observables where dis-connected quark loops do contribute or are even the sole contribution [68]. As said above, our statistics have been often about 150,000 measurements which was necessary to obtain a signal. In fig. 7 we give one example of the isoscalar axial charge of the nucleon g_A^{u+d} . We an-

alyzed g_A^{u+d} both with the standard plateau method and also with the summation method [69, 70, 71] which actually led to the results in fig. 7.

Other examples of nucleon observables are given in ref. [68]. In this paper, in table II, a comprehensive comparison of the contribution of connected and disconnected graphs are listed. One conclusion is that disconnected contributions are clearly important for a number of observables related to nucleon structure. For the sigma terms and scalar charge the disconnected contributions amount to 10% necessitating to take them into account. For the isoscalar axial charge even a larger than 10% contributions is found. Thus, when analyzing the spin carried by quarks in the proton disconnected contributions cannot be neglected. Other quantities where disconnected contributions are significant at the O(10%)-level are Σ^d , the axial form factor G_A and G_p . There are, however, other quantities where dis-connected quark loops provide a negligible contribution. This concerns, e.g. the electromagnetic form factors at low q^2 -values.

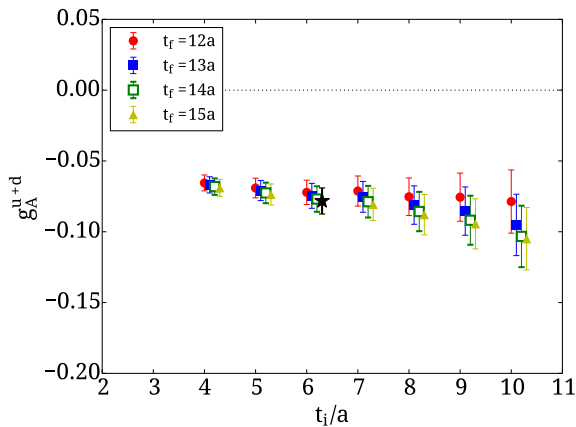


Figure 7: The disconnected contribution to the isoscalar axial charge of the nucleon, g_A^{u+d} . We show results obtained for the fitted slope of the summation method, see ref. [68] for various choices of the initial and final fit time slices as explained in the text.

4.3. Scalar contents of the nucleon

The just discussed dis-connected quark loops are particularly important to address the scalar quark contents of the nucleon. In refs. [72, 56, 73, 74, 75] we have carried out detailed calculation of the scalar light, the strange and also the charm quark contents. For this analysis, we employed gluon configurations for $N_f = 2 + 1 + 1$ flavours [76] of maximally twisted mass fermions which have three advantages for this computation: the first it the automatic $O(a)$ -improvement which allows

to perform a continuum limit in $O(a^2)$. It also leads to very small lattice spacing artefacts, see [75]. The second advantage is that special noise reduction techniques can be used for twisted mass fermions, see [56, 75]. The third advantage is that for maximally twisted mass fermions the mixing in the renormalization process can be avoided [56]. The benefit of these properties allowed us to address for the first time systematic effects that appear in the calculation of the scalar quark contents such as lattice spacing, finite volume and excited state contamination effects.

The quantities computed here are connected to dark matter searches, for which a main observable is the *strangeness of the nucleon*, i.e. the y_N -parameter,

$$y_N \equiv \frac{2\langle N|\bar{s}s|N\rangle}{\langle N|\bar{u}u + \bar{d}d|N\rangle}, \quad (21)$$

where u, d and s are the up, down and strange quark fields.

Direct search experiments for dark matter [77, 78, 79, 80, 81] are based on measuring the recoil energy of a nucleon hit by a dark matter candidate. These experiments can either directly detect a dark matter candidate particle, or, they can provide bounds for models beyond the standard models such as super symmetry [82] or Kaluza-Klein extensions of the standard model [83, 84].

When the interaction of the dark matter particle is mediated through a Higgs boson, the interaction with the nucleon is realized through the scalar quark contents. The spin independent scattering amplitude at zero momentum transfer involves in this case the y_N -parameter. The cross-section is very sensitive on the value of y_N and even small changes in this value can lead to substantial modifications of the cross-section. Thus, it is very important to have a reliable and accurate number for the value of the y_N -parameter. And, since y_N is of non-perturbative nature, a computation from lattice QCD is highly desirable.

Present phenomenological or effective field theory estimates of the y_N -parameter are based on the relation to the ratio of the pion-nucleon ($\sigma_{\pi N}$) and the flavour non-singlet (σ_0) σ -terms, defined as

$$\begin{aligned} \sigma_{\pi N} &\equiv m_l \langle N|\bar{u}u + \bar{d}d|N\rangle, \\ \sigma_s &\equiv m_s \langle N|\bar{s}s|N\rangle \\ \sigma_0 &\equiv m_l \langle N|\bar{u}u + \bar{d}d - 2\bar{s}s|N\rangle \end{aligned} \quad (22)$$

where m_l denotes the average up and down quark mass, and m_s the strange quark mass. With σ_s we denote the strange σ -term. The values of the σ -terms, $\sigma_{\pi N}$ and σ_0 can be estimated by applying chiral effective field

theories using the relation

$$y_N = 1 - \frac{\sigma_0}{\sigma_{\pi N}} \quad (23)$$

from which values of y_N can be calculated.

The way to achieve a value for y_N is to compute $\sigma_{\pi N}$ from the pion nucleon cross section data at an unphysical kinematics, known as the Cheng-Dashen point [85]. There are several analyses, $\sigma_{\pi N} = 45 \pm 8$ MeV from ref. [86] (GLS) and $\sigma_{\pi N} = 64 \pm 7$ MeV from ref. [87] (GWU). Recently, a result has been obtained using baryon covariant chiral perturbation theory in ref. [88] (AMO) which gives $\sigma_{\pi N} = 59 \pm 7$ MeV [88]. The flavour non-singlet σ -term σ_0 can be extracted from the breaking of $SU(3)$ in the spectrum of the octet of baryons. In this way, one finds, see e.g. [89], $\sigma_0^I = 36 \pm 7$ MeV. An alternative way is to use an improved method based on Lorentz covariant chiral perturbation theory with explicit decuplet-baryon resonance fields which gives $\sigma_0^{II} = 58 \pm 8$ MeV [90].

Using the above values for σ_0 different results for the y_N -parameter are obtained. In particular, with σ_0^I one finds

$$\begin{aligned} y_N^{I, \text{GLS}} &= 0.20(21), \quad y_N^{I, \text{GWU}} = 0.44(13) \\ y_N^{I, \text{AMO}} &= 0.39(14). \end{aligned} \quad (24)$$

and with σ_0^{II} ,

$$\begin{aligned} y_N^{II, \text{GLS}} &= -0.29(29), \quad y_N^{II, \text{GWU}} = 0.09(16) \\ y_N^{II, \text{AMO}} &= 0.02(17). \end{aligned} \quad (25)$$

Another analysis [90], derives $y_N = 0.02(13)(10)$ and σ_0 around 60 MeV. The above listed values show a quite large spread leading to correspondingly large uncertainties for the cross-section for dark matter detection, which motivated us to perform a first principle lattice QCD simulation, including light, strange and charm sea quarks with an emphasis on the study of systematic effects.

As a result, we find $y_N = 0.173(50)$. Our result for y_N is compatible with the determinations of refs. [91, 92, 93, 94, 95]. The advantage of our calculation is, however, that systematic effects have been taken into account. The error for y_N originates mainly from systematic uncertainties, in particular the chiral extrapolation and excited state contaminations which cannot be neglected. The chiral extrapolation will be avoided in the future by analyzing gluon field configurations obtained directly at the physical value of the pion mass. However, the error from excited state contaminations is

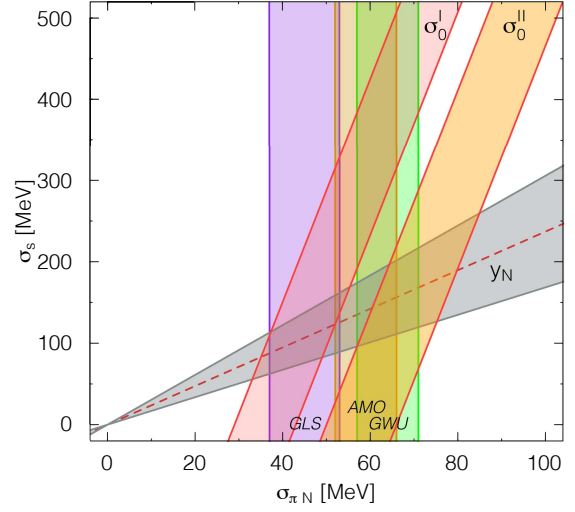


Figure 8: Constraints on σ_s obtained from our determination of y_N . The phenomenological determination of $\sigma_{\pi N}$ are represented by colored band as obtained from [86] (GLS), [87] (GWU) and [88] (AMO). We also show the constraint provided by the estimates σ_0^I [89] and σ_0^{II} [90]. As can be seen the value of y_N can constrain the value of σ_s to be smaller than about 250 MeV.

severe and a systematic analysis is mandatory to reduce the systematic error coming from excited state contaminations.

Our main result, the determination of y_N , leads to a rather low value pointing to an also rather small nucleon-dark matter cross section. As another result, constraints on the σ -terms can be given. Following [96], in fig. 8 the $(\sigma_{\pi N}, \sigma_s)$ plane is shown. We also plot with vertical colored bands phenomenological determinations and the corresponding uncertainties of $\sigma_{\pi N}$. To derive constraints on σ_s , we use the following relations $\sigma_s = \frac{1}{2} \frac{m_s}{m_l} (\sigma_{\pi N} - \sigma_0) = y_N \frac{1}{2} \frac{m_s}{m_l} \sigma_{\pi N}$. The ratio of the quark masses are taken from the FLAG group [97]. The constraints can now be given through the phenomenological value of σ_0 (indicated by σ_0 in fig. 8) and by our direct computation of $y_N = 0.173(50)$ (gray contour) which suggest an upper bound for the strange σ -term of ≈ 250 MeV.

5. Moments of parton distribution functions

The parton distribution functions (PDFs) of quarks and gluons can provide a fascinating insight into the structure of meson and nucleons. Lattice QCD computations can not directly give these parton distribution functions, see however the discussion of a new

approach below. Nevertheless, lattice calculations can provide moments of the PDFs and thus allow for a non-perturbative and first principle analysis of the composition of the bound states that we observe in nature. In addition, with these moments a stringent test of QCD as the theory of the strong interaction can be carried out.

The problem of the lattice calculations in the past has been that simulations were carried through at unphysically large pion masses. In these simulations it was found that many moments do not agree with experimental measurements, e.g. in the case of the nucleon axial charge, or with phenomenological extractions, e.g. for the average quark momentum, see e.g. the reviews [2, 3, 4, 5, 6, 7].

Very fortunately, through substantial algorithmic improvements and significantly enhanced supercomputer power simulations can now be carried out directly at the physical value of the pion mass which allows to avoid the difficulty of extrapolating results to the physical point, see [8, 9, 10, 11].

We report here work performed over a number of years on a systematic analysis of moments of PDFs, quantifying step by step systematic uncertainties, the last one being these chiral extrapolations. Here we want to show the status of the examples of the nucleon scalar, axial and tensor charges and the first moments of the unpolarized, polarized and transversity PDFs. In our work we have employed maximally twisted mass fermions with $N_f = 2$ flavours of mass-degenerate light quarks [98, 54, 99] and also $N_f = 2 + 1 + 1$ flavours [100, 76, 101], including the strange and charm quarks as active degrees of freedom. We will also discuss first results for twisted mass simulations directly at the physical point [35, 36].

Using maximally twisted mass fermions has the invaluable advantage that all physical observables are automatic $O(a)$ -improved. Thus, we do not have to compute any further operator specific improvement coefficients for the rather complicated quantities we need to look at for exploring hadron structure.

To be more specific, we give here the definitions of the first moments of PDFs,

$$\begin{aligned} \langle x \rangle_q &= \int_0^1 dx x [q(x) + \bar{q}(x)], \\ \langle x \rangle_{\Delta q} &= \int_0^1 dx x [\Delta q(x) - \Delta \bar{q}(x)], \\ \langle x \rangle_{\delta q} &= \int_0^1 dx x [\delta q(x) + \delta \bar{q}(x)], \end{aligned} \quad (26)$$

where

$$q(x) = q(x)_\downarrow + q(x)_\uparrow, \quad (27)$$

$$\Delta q(x) = q(x)_\downarrow - q(x)_\uparrow, \quad (28)$$

$$\delta q(x) = q(x)_\perp + q(x)_\top. \quad (29)$$

The moments of eq. (26) can be computed straightforwardly on the lattice, see e.g. [6, 52]. we present in fig. 9 a comparison of the first moments for different collaborations and various quark masses, including the physical point.

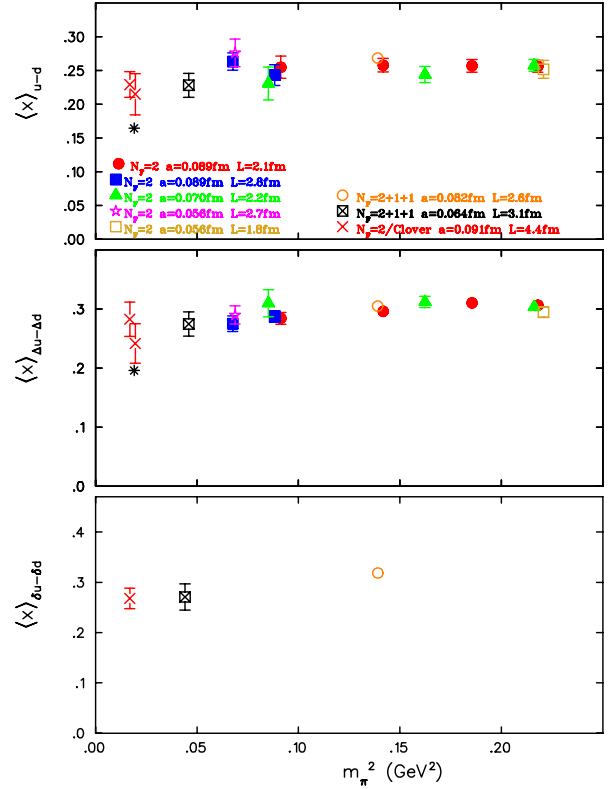


Figure 9: The first iso-vector moments of PDFs, $\langle x \rangle_q$, $\langle x \rangle_{\Delta q}$ and $\langle x \rangle_{\delta q}$. The stars indicate the phenomenological values.

In order to compute the nucleon charges, the operators $\bar{\psi}(x)\frac{\tau^a}{2}\psi(x)$ for the scalar, $\bar{\psi}(x)\gamma^\mu\gamma_5\frac{\tau^a}{2}\psi(x)$ for the axial-vector, and $\bar{\psi}(x)\sigma^{\mu\nu}\frac{\tau^a}{2}\psi(x)$ for the tensor charges have been used.

As already discussed above, for the singlet, isoscalar, axial and tensor nucleon charges g_s^{u+d} , g_A^{u+d} and g_T^{u+d} dis-connected quark loops are required. In refs [53, 68, 66, 102, 103] we have undertaken a dedicated effort to compute these dis-connected contributions, employing a statistics of 150,000 measurements, going thus far beyond state of the art.

The axial and tensor nucleon charges can be extracted to a much better accuracy than the scalar ones such that

they serve as benchmark quantities for hadron structure calculations on the lattice. In fig. 10 we give an overview of the status of these computations, including a simulation at the physical pion mass.

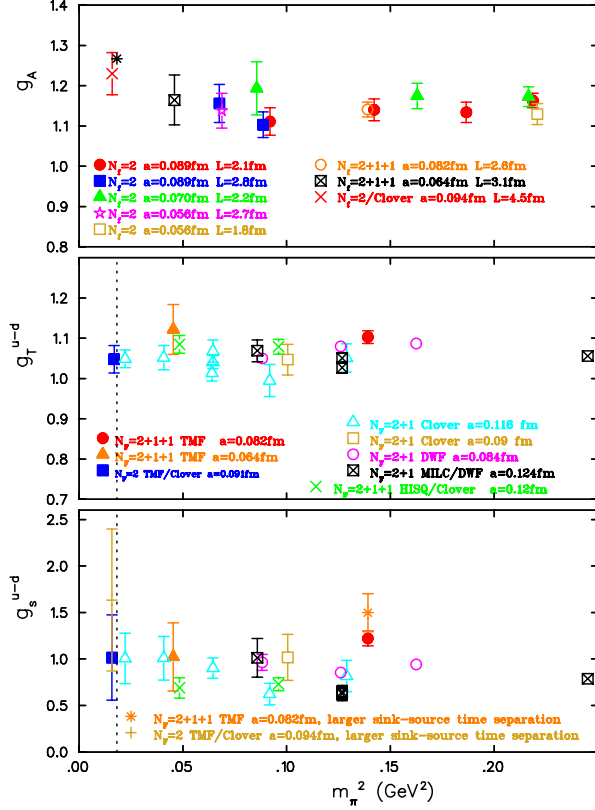


Figure 10: We present the nucleon isovector charges g_A , g_T and g_s and include also a comparison with the results of other collaborations. While for all data the source sink separation is $\sim 1.1 - 1.2$ fm for the orange asterisk and cross for g_s at $m_\pi = 373$ MeV and 130 MeV respectively, the source-sink separation corresponds to ~ 1.5 fm. The stars indicate the experimental or phenomenological values.

As a general conclusion of the above discussed observables relevant for nucleon structure it is fair to say that at the physical pion mass lattice results agree, or, at least tend to agree with experiment and phenomenological evaluations. This provides a very promising perspective. It will be very important to now perform the next steps, i.e. to go to larger volumes to quantify finite size effects and to reach smaller lattice spacings to address lattice spacing artefacts.

5.1. Renormalization

As also reported in the contribution [20] we undertook a dedicated effort to perform a non-perturbative renormalization which is needed for most of the operators relevant for the here discussed hadron structure.

In particular, we looked at the renormalization factor of the one-derivative vector and axial-vector operators, $Z_{DV}^{\mu\nu}$ and $Z_{DA}^{\mu\nu}$. Since they can be classified in two representations we have to distinguish between $Z_{DV}^{\mu\mu}$ ($Z_{DA}^{\mu\mu}$) and $Z_{DV}^{\mu\nu\neq\nu}$ ($Z_{DA}^{\mu\nu\neq\nu}$). The conversion factors from RI-MOM scheme [104] to $\overline{\text{MS}}$ -scheme has been performed using the results of ref. [105] for the local vector and axial-vector operators. For the one-derivative operators the results of ref. [106] were used. For the conversion to the continuum at the commonly used renormalization scale of $(2 \text{ GeV})^2$ we employed perturbation theory at $O(g^4)$. Our results for the renormalization factors can be found in table 5.1.

	$\beta=1.95$	$\beta=2.10$
Z_V	0.625(2)	0.664(1)
Z_A	0.757(3)	0.771(2)
$Z_{DV}^{\mu\mu}$	1.019(4)	1.048(5)
$Z_{DV}^{\mu\nu\neq\nu}$	1.053(11)	1.105(4)
$Z_{DA}^{\mu\mu}$	1.086(3)	1.112(5)
$Z_{DA}^{\mu\nu\neq\nu}$	1.105(2)	1.119(6)

Table 2: Renormalization constants in the chiral limit at $\beta = 1.95$ (corresponding to a lattice spacing of about 0.09fm) and $\beta = 2.10$ (corresponding to a lattice spacing of about 0.075fm) in the $\overline{\text{MS}}$ -scheme at $\mu = 2 \text{ GeV}$.

5.2. Form factors

Besides the moments discussed above, the baryon form factors and their momentum Q^2 dependence is of great importance since also a number of experimental measurements of these form factors have been and will be further carried out. Here we will only show the isovector electric and isovector magnetic form factors, $G_E(Q^2)$ and $G_M(Q^2)$. For a more comprehensive discussion of also other form factors, see ref. [107]. In figs. 11 and 12 we show results for these form factors for pion masses of about 300 MeV. The simulation data were obtained with $N_f = 2 + 1 + 1$ flavours of quarks. The solid line in both graphs represent the parametrization of ref. [108] of experimental data.

There are other collaborations which also compute these form factors, $N_f=2+1$ domain wall fermions [109], $N_f=2$ Wilson improved clover fermions [71] and a hybrid action [110] for a pion mass of about 300 MeV. When we compare to these calculations, a good agreement for the form factors is found, see ref. [107]. This indicates that the discrepancy for the electric form factor is not due using a single action but that this behaviour is more generic.

In [107] we have also varied the pion mass between 370 MeV and 213 MeV. For decreasing pion mass a trend to this description of the experimental data has been found and for the magnetic form factor an agreement with the experimental results was seen for the smallest pion mass of $m_\pi = 213$ MeV. For the electric form factor there is, however, still a discrepancy even at the smallest pion mass. Here a calculation directly at the physical pion mass would be highly desirable in order to see, whether this discrepancy will still remain. Such a calculation is in progress.

The electromagnetic form factors can be fitted using simple dipole ansätze. From such fits the isovector anomalous magnetic moment and root mean square (r.m.s.) radii can be determined. The anomalous magnetic moment is given by the Pauli form factor $F_2(0)$. In the non-relativistic limit the r.m.s. radius is related to the slope of the form factor at zero momentum transfer. Therefore the r.m.s. radii can be obtained from the values of the dipole masses by using

$$\langle r_i^2 \rangle = -\frac{6}{F_i(Q^2)} \frac{dF_i(Q^2)}{dQ^2} \Big|_{Q^2=0} = \frac{12}{m_i^2}, \quad i = 1, 2. \quad (30)$$

These radii again provide a puzzle since they come out to be generally too small when compared to the experimental measurements, see [107]. Thus, the nucleon radii constitute another challenge for lattice QCD calculations and presumably only the simulations at the physical pion mass will finally resolve this puzzle.

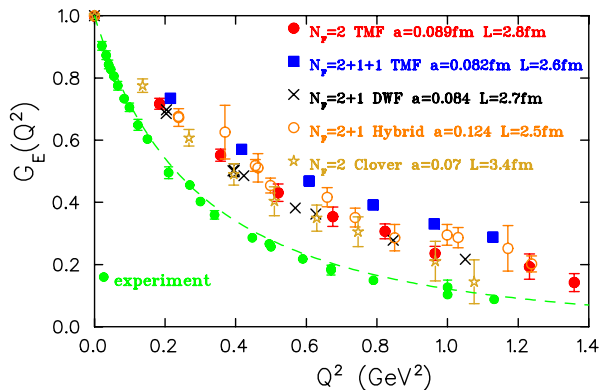


Figure 11: The Q^2 -dependence of $G_E(Q^2)$. We show results for $N_f=2+1+1$ (filled blue squares) and $N_f=2$ [52] (filled red circles) for a pion mass of about 300MeV. We also show results with $N_f=2+1$ domain wall fermions at $m_\pi = 297$ MeV (crosses) [109], with a hybrid action with $N_f=2+1$ staggered sea and DWF at $m_\pi = 293$ MeV (open orange circles) [110], and $N_f=2$ clover at $m_\pi = 290$ MeV (asterisks) [71]. The solid line the parametrization of the experimental data of ref. [108] from a number of experiments as given in Ref. [108].

As another important quantity that can be derived from the form factors is the proton spin, i.e. the ques-

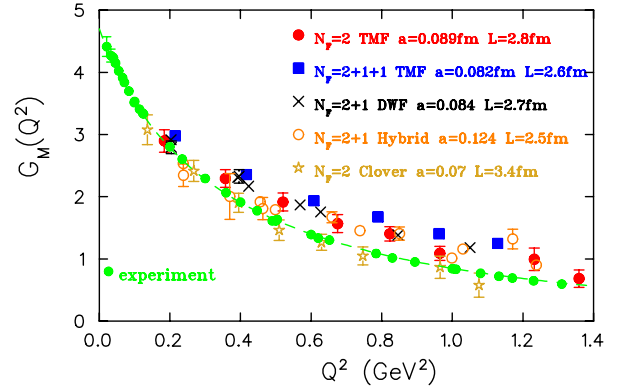


Figure 12: The Q^2 -dependence of the magnetic form factor $G_M(Q^2)$. For the notation see caption of fig. 11.

tion how much of the spin of the proton is carried by the quarks. In particular, from the moments A_{20} and B_{20} one can extract J_q and from g_A the intrinsic spin Σ . Experimentally it is stated that the quarks actually carry only a small fraction [111]. Our understanding today is that it is required to take into account the non-perturbative structure of the proton [112] and lattice QCD calculations are mandatory. First results concerning the proton spin have been obtained, see [107] but the so far required chiral extrapolation for this case is very difficult. However, with the prospect of computing observables relevant for the proton spin at the physical pion mass a very promising perspective is given to obtain the necessary non-perturbative information from lattice QCD computations.

6. Conclusion and outlook

The results presented above are the basic quantities for exploring the structure of hadrons on the lattice, leading to a better understanding of quantum chromodynamics and providing hints for physics beyond the standard model. There are, however, also new approaches that we started within this project and we would like to mention a few of these new, promising directions.

6.1. Gluon moment

A very interesting but extremely difficult to obtain quantity is the first moment of the gluon distribution function, $\langle x \rangle_g$. In fact, only a very small number of computations on the lattice are available which are furthermore performed in the quenched approximation [113, 114]. In ref. [115] we started for the first time a calculation of the gluon moment with active up, down, strange and charm quarks.

For computing the gluon moment the gluon operator

$$O_{\mu\nu} = -\text{tr}_c G_{\mu\rho} G_{\nu\rho} . \quad (31)$$

is needed and we have chosen in particular

$$(\mathcal{B})_{N(p)N(p)} = m_N \langle x \rangle_g , \mathcal{B} = O_{44} - \frac{1}{3} O_{jj} . \quad (32)$$

From this operator and appropriate ratios of 3-point and 2-point functions the desired matrix element can be determined.

We used two different methods to extract the matrix elements. The first is, following [113], the Feynman-Hellman theorem [116] which turned out to be rather difficult, however. The reason is that it has been hard to determine a linear regime of the hadron mass dependence of the gluon matrix element which is required to extract from the slope the first gluon moment.

The second method was a direct computation of the matrix element. Here, a naive approach is almost hopeless, since this matrix element shows a very large noise-to-signal ratio. A solution of the problem is to use HYP smearing [117] for the links in the gluon operator as suggested in [118]. When applying five levels of HYP smearing, using the parameters of [117], we found a significant reduction of the noise-to-signal ratio with increasing number of HYP smearing steps. We have computed the gluon matrix element for three different source-sink separations finding that a plateau is developing, see fig. 13 such that a value of the bare gluon matrix element can be extracted, a result which is clearly promising.

Presently, we are computing in lattice perturbation theory the complicated renormalization of the gluon operator which demands the calculation of a $2 \otimes 2$ renormalization constant matrix due to the mixing with the singlet quark operator. We expect that when this calculation is finished we can provide for the first time an estimate of the first gluon moment in the nucleon in the near future.

6.2. Parton distribution function on the lattice

In this contribution we have discussed moments of PDFs or the Q^2 dependence of nucleon form factors. These quantities are naturally available from lattice QCD computations which are performed in Euclidean time and avoid the problem of going to the light cone. However, there is a new development put forward in ref. [119] which may open a way to determine the PDFs directly on the lattice. In fact, the method has been explored in [120] and first promising results have been found. We have performed also a first analysis of the

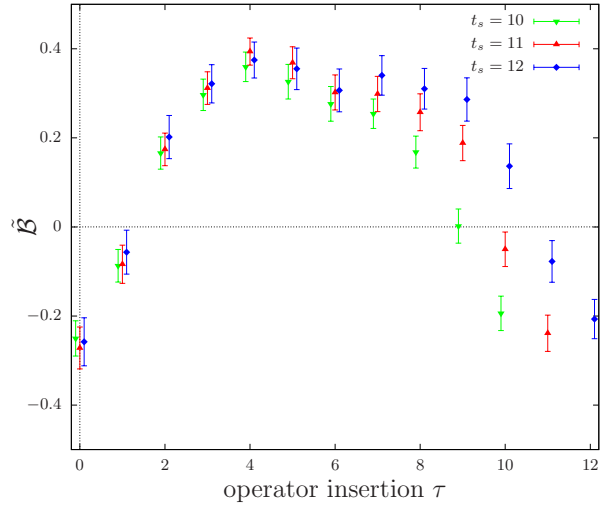


Figure 13: We present the gluon matrix element for a HYP-smearred gluon operator in the nucleon three different source-sink separations. The figure demonstrates that a plateau is developing from which a bare gluon matrix element can be extracted.

approach of [119] using our setup of maximally twisted mass fermions with $N_f = 2 + 1 + 1$ flavours of active quarks.

We refer to ref. [121] for details of our work and mention here only that the method consists of boosting the nucleon on the lattice by providing a momentum in a given direction. In order to render the corresponding operator gauge invariant, a parallel transporter in the direction of the boost is inserted between quark fields. The so defined matrix elements can be related to the PDFs one is actually interested in. To this end, a perturbative matching needs to be performed [122] possibly with target mass corrections [123].

We have already performed a calculation of the lattice matrix elements that needs to be matched to obtain the desired PDFs, see [121]. We have also worked out the matching factor and have the expressions for the target mass corrections. Of course, the approach of computing the PDFs directly leave open a number of questions. One severe aspect is the renormalization of the lattice operator. Another question is, to what momenta one has to go to safely neglect higher order effects in the matching. Despite all these difficulties it is, however, most fascinating that it might be possible to compute PDFs directly on the lattice, an enterprise the lattice community is waiting for since many years.

6.3. Neutron electric dipole moment

As a last topic for a most promising extension of the work presented here, we want to mention the neutron

electric dipole moment (nEDM). This dipole moment is related to the phenomenon of CP-violation and is predicted to be very small in the standard model. However, when looking at models beyond the standard model, the neutron electric dipole moment can be much larger and hence having a solid prediction for the dipole moment from first principles lattice QCD calculations is highly desirable. In refs. [124, 125] the CP violating operators have been classified and the mixing and renormalization have been discussed. One important ingredient in the calculation of the neutron electric dipole moment is the knowledge of the topological charge, see [126, 127] for a recent comparison of different topological charge definitions.

Our collaboration has setup all ingredients for a computation of the neutron electric dipole moment with maximally twisted mass fermions. At the moment we are performing test runs but we expect to have results for the dipole moment in the near future. Clearly, without the preparatory work on hadron structure described in this proceedings such a calculation would not have been possible.

6.4. Summary

In this contribution we have demonstrated that nowadays lattice QCD simulations for exploring the masses and the structure of hadrons can be performed at the physical value of the pion mass. This breakthrough that which has been achieved in this project shows a promising tendency that at the physical point older discrepancies between lattice results and those from experiment or phenomenology can be resolved.

Performing further improvements to quantify the systematic effects of a finite volume and a non-zero lattice spacing together with a better analysis of excited state and dis-connected quark loop contributions will put lattice QCD in a unique position to reveal the structure of hadrons and, in case of significant discrepancies, to point to physics beyond the standard model.

Acknowledgment

The results on the hadron masses and structure presented here would not have been possible without the great work and help of many people, i.e. K. Cichy, M. Constantinou, S. Dinter, V. Drach, E. Garcia-Ramos, K. Hadjiyiannakou, C. Kallidonis, G. Koutsou, M. Papinutto, D. Renner, A. Shindler, F. Steffens, C. Urbach, A. Vaquero, I. Wetzorke, C. Wiese. We most gratefully acknowledge these people for a most enjoyable and fruitful collaboration and for the many important contributions they provided.

- [1] R. Devenish and A. Cooper-Sarkar, (2004).
- [2] P. Hagler, Phys.Rept. **490**, 49 (2010), arXiv:0912.5483 [hep-lat].
- [3] D. Boer *et al.*, arXiv:1108.1713 [nucl-th].
- [4] C. Alexandrou, PoS **LATTICE2010**, 001 (2010), arXiv:1011.3660 [hep-lat].
- [5] D. B. Renner, PoS **LAT2009**, 018 (2009), arXiv:1002.0925 [hep-lat].
- [6] C. Alexandrou *et al.*, Phys.Rev. **D83**, 094502 (2011), arXiv:1102.2208 [hep-lat].
- [7] S. Collins *et al.*, Phys.Rev. **D84**, 074507 (2011), arXiv:1106.3580 [hep-lat].
- [8] C. Alexandrou *et al.*, Nuovo Cim. **C036**, 111 (2013), arXiv:1303.6818 [hep-lat].
- [9] C. Alexandrou, EPJ Web Conf. **73**, 01013 (2014), arXiv:1404.5213 [hep-lat].
- [10] S. Syritsyn, PoS **LATTICE2013**, 009 (2014), arXiv:1403.4686 [hep-lat].
- [11] M. Constantinou, PoS **LATTICE2014**, 001 (2014), arXiv:1411.0078 [hep-lat].
- [12] A. De Freitas and J. Blümlein, this proceedings.
- [13] C. Best *et al.*, Phys.Rev. **D56**, 2743 (1997), arXiv:hep-lat/9703014 [hep-lat].
- [14] M. Guagnelli, K. Jansen and R. Petronzio, Nucl.Phys. **B542**, 395 (1999), arXiv:hep-lat/9809009 [hep-lat].
- [15] M. Guagnelli, K. Jansen and R. Petronzio, Phys.Lett. **B457**, 153 (1999), arXiv:hep-lat/9901016 [hep-lat].
- [16] M. Guagnelli, K. Jansen and R. Petronzio, Phys.Lett. **B493**, 77 (2000), arXiv:hep-lat/0009006 [hep-lat].
- [17] **Zeuthen-Rome / ZeRo Collaboration** Collaboration, M. Guagnelli *et al.*, Nucl.Phys. **B664**, 276 (2003), arXiv:hep-lat/0303012 [hep-lat].
- [18] **Zeuthen-Rome (ZeRo) Collaboration** Collaboration, M. Guagnelli *et al.*, Phys.Lett. **B597**, 216 (2004), arXiv:hep-lat/0403009 [hep-lat].
- [19] **Zeuthen-Rome (ZeRo) Collaboration** Collaboration, M. Guagnelli *et al.*, Eur.Phys.J. **C40**, 69 (2005), arXiv:hep-lat/0405027 [hep-lat].
- [20] K. Jansen, this proceedings.
- [21] R. Frezzotti and G. C. Rossi, JHEP **08**, 007 (2004), hep-lat/0306014.
- [22] S. Capitani *et al.*, Phys.Lett. **B639**, 520 (2006), arXiv:hep-lat/0511013 [hep-lat].
- [23] M. Baake, B. Gemunden and R. Odingen, J.Math.Phys. **24**, 1021 (1983).
- [24] J. E. Mandula, G. Zweig and J. Govaerts, Nucl.Phys. **B228**, 91 (1983).
- [25] G. Martinelli and C. T. Sachrajda, Phys.Lett. **B196**, 184 (1987).
- [26] M. Luscher, R. Narayanan, P. Weisz and U. Wolff, Nucl.Phys. **B384**, 168 (1992), arXiv:hep-lat/9207009 [hep-lat].
- [27] S. Sint, Nucl.Phys. **B421**, 135 (1994), arXiv:hep-lat/9312079 [hep-lat].
- [28] S. Sint, Nucl.Phys. **B451**, 416 (1995), arXiv:hep-lat/9504005 [hep-lat].
- [29] K. Jansen *et al.*, Phys.Lett. **B372**, 275 (1996), arXiv:hep-lat/9512009 [hep-lat].
- [30] P. Sutton, A. D. Martin, R. Roberts and W. J. Stirling, Phys.Rev. **D45**, 2349 (1992).
- [31] M. Gluck, E. Reya and I. Schienbein, Eur.Phys.J. **C10**, 313 (1999), arXiv:hep-ph/9903288 [hep-ph].
- [32] K. Wijesooriya, P. Reimer and R. Holt, Phys.Rev. **C72**, 065203 (2005), arXiv:nucl-ex/0509012 [nucl-ex].
- [33] C. Urbach, K. Jansen, A. Shindler and U. Wenger, Comput. Phys. Commun. **174**, 87 (2006), hep-lat/0506011.

- [34] K. Jansen and C. Urbach, *Comput.Phys.Commun.* **180**, 2717 (2009), arXiv:0905.3331 [hep-lat].
- [35] A. Abdel-Rehim *et al.*, PoS **LATTICE2013**, 264 (2013), arXiv:1311.4522 [hep-lat].
- [36] A. Abdel-Rehim *et al.*, PoS **LATTICE2014**, 119 (2014), arXiv:1411.6842 [hep-lat].
- [37] C. Alexandrou, V. Drach, K. Jansen, C. Kallidonis and G. Koutsou, arXiv:1406.4310 [hep-lat].
- [38] **European Twisted Mass Collaboration** Collaboration, C. Alexandrou *et al.*, *Phys.Rev.* **D78**, 014509 (2008), arXiv:0803.3190 [hep-lat].
- [39] **ETM Collaboration** Collaboration, C. Alexandrou *et al.*, *Phys.Rev.* **D80**, 114503 (2009), arXiv:0910.2419 [hep-lat].
- [40] S. Prelovsek, PoS **LATTICE2014**, 015 (2014), arXiv:1411.0405 [hep-lat].
- [41] **Particle Data Group** Collaboration, K. Hagiwara *et al.*, *Phys.Rev.* **D66**, 010001 (2002).
- [42] H. Na and S. A. Gottlieb, PoS **LAT2007**, 124 (2007), arXiv:0710.1422 [hep-lat].
- [43] H. Na and S. Gottlieb, PoS **LATTICE2008**, 119 (2008), arXiv:0812.1235 [hep-lat].
- [44] R. A. Briceño, H.-W. Lin and D. R. Bolton, *Phys.Rev.* **D86**, 094504 (2012), arXiv:1207.3536 [hep-lat].
- [45] L. Liu, H.-W. Lin, K. Orginos and A. Walker-Loud, *Phys.Rev.* **D81**, 094505 (2010), arXiv:0909.3294 [hep-lat].
- [46] **PACS-CS Collaboration** Collaboration, Y. Namekawa *et al.*, *Phys.Rev.* **D87**, 094512 (2013), arXiv:1301.4743 [hep-lat].
- [47] S. Dinter *et al.*, *Phys.Lett.* **B704**, 89 (2011), arXiv:1108.1076 [hep-lat].
- [48] S. Dinter *et al.*, PoS **LATTICE2010**, 135 (2010), arXiv:1101.5540 [hep-lat].
- [49] **Particle Data Group** Collaboration, K. Nakamura *et al.*, *J.Phys.* **G37**, 075021 (2010).
- [50] S. Alekhin, J. Blumlein, S. Klein and S. Moch, *Phys.Rev.* **D81**, 014032 (2010), arXiv:0908.2766 [hep-ph].
- [51] **ETM Collaboration** Collaboration, C. Alexandrou *et al.*, *Phys.Rev.* **D83**, 045010 (2011), arXiv:1012.0857 [hep-lat].
- [52] C. Alexandrou *et al.*, *Phys.Rev.* **D83**, 114513 (2011), arXiv:1104.1600 [hep-lat].
- [53] C. Alexandrou *et al.*, *Comput.Phys.Commun.* **185**, 1370 (2014), arXiv:1309.2256 [hep-lat].
- [54] **ETM Collaboration**, P. Boucaud *et al.*, *Comput.Phys.Commun.* **179**, 695 (2008), arXiv:0803.0224 [hep-lat].
- [55] **ETM Collaboration**, C. Michael and C. Urbach, PoS **LAT2007**, 122 (2007), arXiv:0709.4564 [hep-lat].
- [56] **ETM Collaboration** Collaboration, S. Dinter *et al.*, *JHEP* **1208**, 037 (2012), arXiv:1202.1480 [hep-lat].
- [57] S. Bernardson, P. McCarty and C. Thron, *Comput.Phys.Commun.* **78**, 256 (1993).
- [58] **TXL Collaboration** Collaboration, J. Viehoff *et al.*, *Nucl.Phys.Proc.Suppl.* **63**, 269 (1998), arXiv:hep-lat/9710050 [hep-lat].
- [59] **TrinLat Collaboration** Collaboration, A. O’Cais, K. J. Juge, M. J. Peardon, S. M. Ryan and J.-I. Skullerud, arXiv:hep-lat/0409069 [hep-lat].
- [60] J. Foley *et al.*, *Comput.Phys.Commun.* **172**, 145 (2005), arXiv:hep-lat/0505023 [hep-lat].
- [61] C. Alexandrou, K. Hadjiyiannakou, G. Koutsou, A. O’Cais and A. Strelchenko, *Comput.Phys.Commun.* **183**, 1215 (2012), arXiv:1108.2473 [hep-lat].
- [62] S. Collins, G. Bali and A. Schafer, PoS **LAT2007**, 141 (2007), arXiv:0709.3217 [hep-lat].
- [63] G. S. Bali, S. Collins and A. Schafer, *Comput.Phys.Commun.* **181**, 1570 (2010), arXiv:0910.3970 [hep-lat].
- [64] **UKQCD Collaboration** Collaboration, C. McNeile and C. Michael, *Phys.Rev.* **D63**, 114503 (2001), arXiv:hep-lat/0010019 [hep-lat].
- [65] A. Strelchenko, C. Alexandrou, G. Koutsou and A. V. Aviles-Casco, arXiv:1311.4462 [hep-lat].
- [66] C. Alexandrou, K. Hadjiyiannakou, G. Koutsou, A. Strelchenko and A. V. Aviles-Casco, PoS **LATTICE2013**, 411 (2014), arXiv:1401.6750 [hep-lat].
- [67] V. Azcoiti, E. Follana, A. Vaquero and G. Di Carlo, *JHEP* **0908**, 008 (2009), arXiv:0905.0639 [hep-lat].
- [68] A. Abdel-Rehim *et al.*, *Phys.Rev.* **D89**, 034501 (2014), arXiv:1310.6339 [hep-lat].
- [69] L. Maiani, G. Martinelli, M. Paciello and B. Taglienti, *Nucl.Phys.* **B293**, 420 (1987).
- [70] S. Gusken, arXiv:hep-lat/9906034 [hep-lat].
- [71] S. Capitani, B. Knippschild, M. Della Morte and H. Wittig, PoS **LATTICE2010**, 147 (2010), arXiv:1011.1358 [hep-lat].
- [72] S. Dinter, V. Drach and K. Jansen, *Int.J.Mod.Phys.Proc.Suppl.* **E20**, 110 (2011), arXiv:1111.5426 [hep-lat].
- [73] C. Alexandrou *et al.*, PoS **LATTICE2012**, 163 (2012), arXiv:1211.4447 [hep-lat].
- [74] C. Alexandrou *et al.*, PoS **LATTICE2013**, 295 (2013), arXiv:1311.6132 [hep-lat].
- [75] C. Alexandrou *et al.*, arXiv:1309.7768 [hep-lat].
- [76] **ETM Collaboration**, R. Baron *et al.*, *JHEP* **1006**, 111 (2010), arXiv:1004.5284 [hep-lat].
- [77] **CDMS-II Collaboration** Collaboration, Z. Ahmed *et al.*, *Phys.Rev.Lett.* **106**, 131302 (2011), arXiv:1011.2482 [astro-ph.CO].
- [78] **DAMA Collaboration** Collaboration, R. Bernabei *et al.*, *Eur.Phys.J.* **C56**, 333 (2008), arXiv:0804.2741 [astro-ph].
- [79] **CoGeNT collaboration** Collaboration, C. Aalseth *et al.*, *Phys.Rev.Lett.* **106**, 131301 (2011), arXiv:1002.4703 [astro-ph.CO].
- [80] **ZEPLIN-III Collaboration** Collaboration, T. Sumner, *AIP Conf.Proc.* **1200**, 963 (2010).
- [81] J. Jochum *et al.*, *Prog.Part.Nucl.Phys.* **66**, 202 (2011).
- [82] J. Ellis and K. A. Olive, arXiv:1001.3651 [astro-ph.CO].
- [83] G. Servant and T. M. Tait, *New J.Phys.* **4**, 99 (2002), arXiv:hep-ph/0209262 [hep-ph].
- [84] G. Bertone, K. Kong, R. R. de Austri and R. Trotta, *Phys.Rev.* **D83**, 036008 (2011), arXiv:1010.2023 [hep-ph].
- [85] T. Cheng and R. F. Dashen, *Phys.Rev.Lett.* **26**, 594 (1971).
- [86] J. Gasser, H. Leutwyler and M. Sainio, *Phys.Lett.* **B253**, 252 (1991).
- [87] M. Pavan, I. Strakovsky, R. Workman and R. Arndt, *PiN Newsllett.* **16**, 110 (2002), arXiv:hep-ph/0111066 [hep-ph].
- [88] J. Alarcon, J. Martin Camalich and J. Oller, *Phys.Rev.* **D85**, 051503 (2012), arXiv:1110.3797 [hep-ph].
- [89] B. Borasoy and U.-G. Meissner, *Annals Phys.* **254**, 192 (1997), arXiv:hep-ph/9607432 [hep-ph].
- [90] J. Alarcon, L. Geng, J. Martin Camalich and J. Oller, *Phys.Lett.* **B730**, 342 (2014), arXiv:1209.2870 [hep-ph].
- [91] **QCDSF Collaboration** Collaboration, G. S. Bali *et al.*, *Phys.Rev.* **D85**, 054502 (2012), arXiv:1111.1600 [hep-lat].
- [92] S. Durr *et al.*, *Phys.Rev.* **D85**, 014509 (2012), arXiv:1109.4265 [hep-lat].

- [93] **QCDSF-UKQCD Collaborations** Collaboration, R. Horsley *et al.*, Phys.Rev. **D85**, 034506 (2012), arXiv:1110.4971 [hep-lat].
- [94] R. Young and A. Thomas, Phys.Rev. **D81**, 014503 (2010), arXiv:0901.3310 [hep-lat].
- [95] P. Shanahan, A. Thomas and R. Young, Phys.Rev. **D87**, 074503 (2013), arXiv:1205.5365 [nucl-th].
- [96] R. Young, PoS **LATTICE2012**, 014 (2012), arXiv:1301.1765 [hep-lat].
- [97] G. Colangelo *et al.*, Eur.Phys.J. **C71**, 1695 (2011), arXiv:1011.4408 [hep-lat].
- [98] **ETM** Collaboration, P. Boucaud *et al.*, Phys. Lett. **B650**, 304 (2007), arXiv:hep-lat/0701012.
- [99] **ETM** Collaboration, R. Baron *et al.*, JHEP **1008**, 097 (2010), arXiv:0911.5061 [hep-lat].
- [100] T. Chiarappa *et al.*, Eur.Phys.J. **C50**, 373 (2007), arXiv:hep-lat/0606011 [hep-lat].
- [101] **European Twisted Mass Collaboration** Collaboration, R. Baron *et al.*, Comput.Phys.Commun. **182**, 299 (2011), arXiv:1005.2042 [hep-lat].
- [102] C. Alexandrou, V. Drach, K. Jansen, G. Koutsou and A. V. Avils-Casco, PoS **LATTICE2013**, 270 (2014), arXiv:1401.6749 [hep-lat].
- [103] C. Alexandrou *et al.*, arXiv:1411.3494 [hep-lat].
- [104] G. Martinelli, C. Pittori, C. T. Sachrajda, M. Testa and A. Vladikas, Nucl. Phys. **B445**, 81 (1995), arXiv:hep-lat/9411010.
- [105] J. Gracey, Nucl.Phys. **B662**, 247 (2003), arXiv:hep-ph/0304113 [hep-ph].
- [106] C. Alexandrou, M. Constantinou, T. Korzec, H. Panagopoulos and F. Stylianou, Phys.Rev. **D83**, 014503 (2011), arXiv:1006.1920 [hep-lat].
- [107] C. Alexandrou *et al.*, Phys.Rev. **D88**, 014509 (2013), arXiv:1303.5979 [hep-lat].
- [108] J. Kelly, Phys.Rev. **C70**, 068202 (2004).
- [109] S. Syritsyn *et al.*, Phys.Rev. **D81**, 034507 (2010), arXiv:0907.4194 [hep-lat].
- [110] **LHPC Collaboration** Collaboration, J. Bratt *et al.*, Phys.Rev. **D82**, 094502 (2010), arXiv:1001.3620 [hep-lat].
- [111] **European Muon Collaboration** Collaboration, J. Ashman *et al.*, Phys.Lett. **B206**, 364 (1988).
- [112] A. W. Thomas, Int.J.Mod.Phys. **E18**, 1116 (2009), arXiv:0904.1735 [hep-ph].
- [113] **QCDSF Collaboration, UKQCD Collaboration** Collaboration, R. Horsley *et al.*, Phys.Lett. **B714**, 312 (2012), arXiv:1205.6410 [hep-lat].
- [114] K. Liu *et al.*, PoS **LATTICE2011**, 164 (2011), arXiv:1203.6388 [hep-ph].
- [115] C. Alexandrou *et al.*, PoS **LATTICE 2013**, 289 (2013), arXiv:1311.3174 [hep-lat].
- [116] R. Feynman, Phys.Rev. **56**, 340 (1939).
- [117] A. Hasenfratz and F. Knechtli, Phys. Rev. **D64**, 034504 (2001), hep-lat/0103029.
- [118] H. B. Meyer and J. W. Negele, Phys.Rev. **D77**, 037501 (2008), arXiv:0707.3225 [hep-lat].
- [119] X. Ji, Phys.Rev.Lett. **110**, 262002 (2013), arXiv:1305.1539 [hep-ph].
- [120] H.-W. Lin, J.-W. Chen, S. D. Cohen and X. Ji, arXiv:1402.1462 [hep-ph].
- [121] C. Alexandrou *et al.*, PoS **LATTICE2014**, 135 (2014), arXiv:1411.0891 [hep-lat].
- [122] X. Xiong, X. Ji, J.-H. Zhang and Y. Zhao, Phys.Rev. **D90**, 014051 (2014), arXiv:1310.7471 [hep-ph].
- [123] F. Steffens, M. Brown, W. Melnitchouk and S. Sanches, Phys.Rev. **C86**, 065208 (2012), arXiv:1210.4398 [hep-ph].
- [124] T. Bhattacharya, V. Cirigliano and R. Gupta, PoS **LATTICE2012**, 179 (2012), arXiv:1212.4918.
- [125] T. Bhattacharya, V. Cirigliano and R. Gupta, PoS **LATTICE2013**, 299 (2014), arXiv:1403.2445 [hep-lat].
- [126] M. Mller-Preussker, to appear in PoS .
- [127] K. Cichy *et al.*, PoS **LATTICE2014**, 075 (2014), arXiv:1411.1205 [hep-lat].